New Routes Towards Formation of Tin Oxide Inverted Opals for Charge Storage Applications

M. Osiak[1], E. Armstrong[1], and C. O'Dwyer[1,2,3]

[1]*Department of Chemistry, University College Cork, Cork, Ireland*
[2] *Materials and Surface Science Institute, University of Limerick, Limerick, Ireland*
[3] *Micro & Nanoelectronics Centre, Tyndall National Institute, Dyke Parade, Cork, Ireland*

New routes to formation of tin oxide inverted opals with unique morphologies are presented. Inverted opals with walls formed from assemblies of tin oxide nanocrystals are formed from tin acetate precursor, while mesoporous walls are formed when tin alkoxide precursors are used. The inverted opals are investigated by a variety of techniques in order to determine their structure and the dependence of electrochemical properties on the type of precursor used. We found that the initial discharge capacity of the inverted opal based batteries reaches 1200 $mAhg^{-1}$ but quickly fades afterwards, as it is typical for tin oxide based anodes. Careful investigation of processes occurring in the tin oxide inverted opal anodes may lead to improvement of their performance improvement, and further development of self-supported tin oxide based anodes.

Introduction

New generation energy storage mechanisms will require a balance between energy density and power density. The optimisation of both of these parameters led to extensive research into advanced battery architectures and materials (1). Super-capacitors (2), fuel cells (3), and different types of battery chemistries have all been considered as a possible solution to long term sustainable energy storage. Among those chemistries, lithium ion batteries are the most promising due to combination of greater specific energy density and specific power density than other battery types. The mechanism of charge storage in lithium ion batteries is well known and consists of intercalation of lithium ion into the lattice of crystalline solid or vacancies in disordered host. The factor limiting the rate of this reaction is related to low diffusivity of lithium in currently used materials, which limits the rates at which the batteries can be charged or discharged (4). A variety of options for improving the rate performance is available, and involves, but is not limited to, decreasing the size of the active material (1, 5, 6), introducing conductive additives and rationally designing electrode architecture (7, 8). The decreasing size of the active material in particular can provide solution to the problem of low rate capability, by resolving low diffusivity of lithium ions in host materials. If one of useful dimensions of the material is smaller than specific diffusion length of lithium ion in the host material, then the rate capability can be greatly improved. This combined with rational electrode design should allow batteries with performance capabilities greatly exceeding currently observed ones.

To further improve the performance of the battery electrode, the use of rationally designed 3-dimensional electrode architectures has been extensively investigated. Approaches such as interdigitated electrodes (9) (both in tubular and planar form), sponge geometries (9),

and inverted opal (IO) structures (10) offer way to vary the type and degree of porosity. Inverted opals in particular offer great control over the pore size, and geometry as well as allowing formation of electrodes from a variety of materials due to simple wet chemical based processing (11). Three-dimensional ordered mesoporous structures such as IOs have been extensively investigated for applications in photonics or gas sensing (12) and due to their large surface area combined with precise control over structure, they may be applied in lithium ion batteries both as cathodes and anodes. In fact, recent demonstration of 3DOM based microbattery proves that this approach has great practical advantages (13-15). Before the IO electrodes are used in real life batteries however, more investigation needs to be carried out in order to better understand the processes occurring in the electrode, the dependence of the precursors used on the electrode performance as well as the structure of the IO itself.

Another important consideration for next generation batteries are materials used for cathode and anode. For anode in particular, metals and their oxides that can alloy with lithium are promising due to their larger specific capacities compared to graphite. For instance, Silicon (4400 mAh g^{-1} (16)) Germanium (1400 mAh g^{-1}(17)) or Sn (1000 mAh g^{-1} (18)) are able to store significantly more charge per unit weight than currently used graphite (372 mAh g^{-1}). The drawback associated with storage of such high lithium amounts is extreme volumetric expansion of the electrode material. This leads to loss of mechanical integrity of electrodes and subsequent decrease in the battery capacity. Strategies such as decreasing size of active material below certain critical value or providing mechanical buffers for mechanical expansions of active material species have been both used to improve the electrochemical performance of alloying anodes.

In this paper, we present a novel approach to formation of a series tin oxide IO battery anodes with different nanoscale morphologies and degrees of hierarchical porosity. We use electrophoretic deposition to form large size electrode templates of polymeric sphere assemblies each infilled with a range of inorganic precursors to crystallize the tin oxide IO structures. The influence of the type of the precursor on the nanoscale morphology, pore structure and effective porosity and the electrochemical performance of the IO based anodes was investigated by a variety of electrochemical and analytical techniques.

Experimental

Polystyrene sphere template preparation

Polystyrene spheres were prepared by emulsion polymerization procedure described elsewhere (19). Briefly, sodium lauryl sulphate and potassium persulfate were dissolved in aqueous ethanol in a 250 ml three-neck round bottom flask. A fixed quantity of styrene was then added under nitrogen atmosphere and rapid stirring and the emulsion solution was heated to 70 °C to polymerize for 8 h. Prior to use the styrene was washed with 10% sodium hydroxide in a separator funnel in order to remove the polymerization inhibitor.

Electrophoretic deposition

Electrophoretic deposition was used to prepare large scale opal templates with great degree of ordering. Briefly, 0.8 ml of spheres dispersed in water were mixed with 3.2 ml of ethanol to form 4 ml of solution with 1.25% spheres concentration. To adjust the pH of the mixture to ~10, ammonium hydroxide was added to the solution. The electrodes (stainless steel foil, 0.6 × 6cm) were washed in acetone, ethanol, and deionized water by sonication to ensure removal of all organic and inorganic impurities from their surface. The electrodes were kept at a constant distance of 5 mm from each other and were kept completely in parallel. The electrophoretic deposition was carried out at 2.5 V applied for at least 20 minutes. Following that, a short 5 second 150 V pulse was applied to the electrodes to ensure their mechanical integrity of the

deposited spheres. The templates were dried in air overnight and used for depositions without any further treatment.

IO preparation

Inverted opals were prepared by direct infiltration of the opal templates and subsequent removal of the template material. Briefly, tin oxide precursors (tin acetate (II) tin acetate (IV) tin ethylhexano-isopropoxide and tin isopropoxide were mixed with a suitable solvent and directly applied to the opal template. Following the precursor application, the templates were placed in vacuum for at least 30 minutes in order to ensure complete infiltration of the templates by the precursor. The templates were then dried in the oven for at least 2 hours at 40 °C to ensure complete evaporation of the solvent. To remove the polystyrene spheres, the infiltrated opal template was then placed in the oven at 500 °C for 5 hours. After the deposition the prepared inverted opals were characterized by a variety of techniques.

Sample characterization

Inverted opal samples were characterized by a variety of techniques. Scanning electron microscopy (SEM) images were collected on a FEI Quanta 650 microscope operating at 10 kV and transmission electron microscopy (TEM) images were collected on a JEOL JEM 2100 TEM operating at 200 kV. For electrochemical measurements, samples were placed in stainless-steel half cells. Lithium foil (MTI Corporation) was used as counter and reference electrodes and. Glass fibre separator (Whatmann) was soaked in the electrolyte consisting of $LiPF_6$ dissolved in 1 mol dm^{-3} EC:DMC at 1:1v/v ratio. Electrochemical measurements were carried out using Bio-Logic VSP potentiostat, operating between 0 – 2.5 V in case of CVs and 0 – 3 V in the case of galvanostatic measurements. After cycling the samples were removed from the cells and carefully washed in acetonitrile and 10^{-4} mol dm^{-3} acetic acid to remove the electrolyte residue.

Results and discussion

Tin oxide IOs were prepared by infiltration of the opal template prepared by electrophoretic deposition (see Figure 1a for the schematic of the sample preparation). The PS spheres, synthesized with a diameter of 750 ± 15 nm were deposited in a rapid and reproducible experiment with a high degree of packing order. Excellent long range order of the self-assembled sphere template is also found using this approach owing to the monodispersity of sphere sizes and carefully tailored experimental conditions. Figure 1b shows the surface of as-prepared template. The order of the spheres is clearly visible, with the (111) face of the effectively cubic arrangement parallel to the substrate. Usually, in the preparation of opal templates, the (111) plane forms preferentially to other planes due to lowest energy (maximum packing) for the spheres in this arrangement (20-22). Increasing temperature or changing deposition conditions can also allow for other planes to crystallize (for instance {110} or {100}). Here, we notice that {110} planes can coexist with {111} planes that form during the electrophoretic deposition step. This is likely attributed to the high rate of deposition of the spheres on the substrate (compared to Langmuir-Blodgett layer-by-layer deposition of from slower μm/min dipping deposition) which prevents them from minimizing their energy and packing into a hexagonal arrangement.

The crystalline template is formed from multiple crystalline grains. Defects typical for opal templates can also be observed on the surface of the samples (see Figure 1b). Edge dislocations and point defects show in most opal templates, and although undesirable in photonics are of little consequence for charge storage applications as they do not affect electrochemical properties of the prepared structure.

After the template preparation, the template spheres are soaked in tin oxide precursor. The precursors used were dissolved in a solvent that would penetrate the voids between the spheres (ethanol for tin acetates or 2 methxy ethanol in case of alkoxides). Vacuum was applied to ensure complete penetration of the opal template by the precursor to infill the opal template down to the substrate interface. Application of vacuum to assist the penetration opal templates ensures formation of uniform inverted opal structures, as opposed to thin film overlayers that may form on the surface of the opal template. Compared to other infiltration methods such as CVD or electrodeposition, vacuum-assisted infiltration offers the advantage of simplicity and low cost, which is desirable for upscaled charge storage applications.

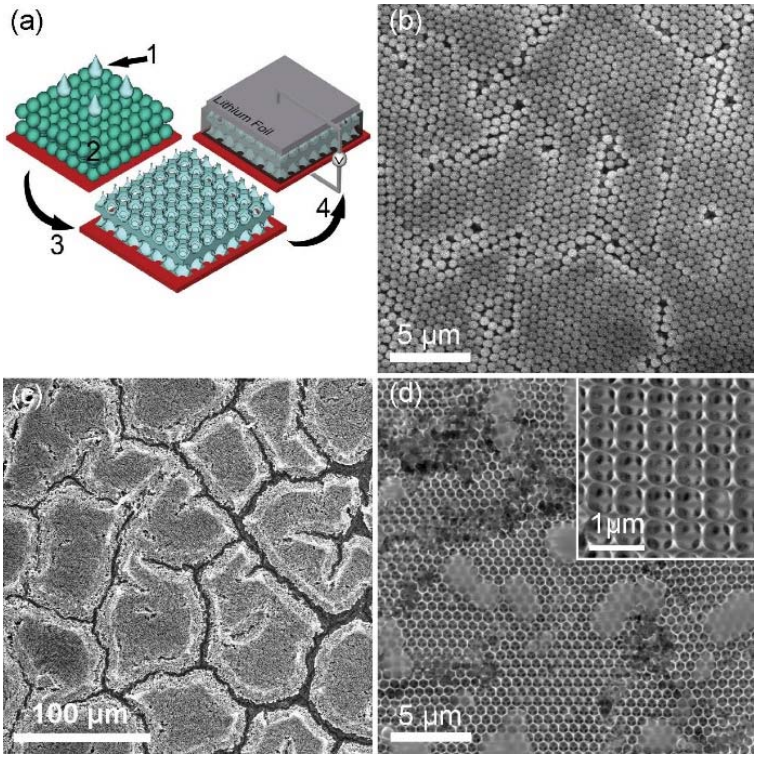

Figure 1. (a) Schematic diagram depicting IO structure formation. (b) SEM image of polystyrene spheres forming opal template. (c) Low magnification SEM image presenting surface of the IO. Large degree of cracking and porosity is clearly visible. (d) High magnification SEM image showing the (111) orientation of the IO structure. The inset shows the IO structure in the (110) orientation.

To remove the opal template, the infiltrated samples were placed in an oven in oxygen atmosphere at 500 °C. During this calcination, polystyrene spheres are decomposed leaving inverted opal structures of precursor. Additionally, the high temperature of the template removal accelerates the process of hydrolysis of the tin oxide precursor and crystallization of IO walls. A macroscle SEM image of the as-formed inverted opal is showed in a Figure 1c. As the porous material forms, characteristic cracking occurs. This is due to the removal of solvent and liquids from a porous materials, which typically results in shrinkage. Additionally, the volume of the precursor changes as the organic moieties are decomposed and removed and the material crystallizes to SnO_2. The crystallographic or geometrical order of the inverted opal generally follows that of the template areas; the decomposition step does not adversely affect the packing arrangement defined by the template (Fig. 1d). There are also certain areas where the order is not clearly distinguishable. This type of structure, where there is no order present is called a photonic glass.

The type of the precursor used has a significant influence on the morphology of the walls that make up the inverted opals. In the case of tin acetate-based inverted opal, the wall consists of an assembly of tin oxide nanoparticles. A number of grain boundaries is clearly distinguishable in low magnification TEM image in Fig. 2a. The nanoparticles fill up the voids between the template spheres forming continuous 3-dimensional structures. This can be attributed to the process of recrystallization of tin oxide from tin acetate. Using an alkoxide based precursor results in formation of an inverted opal structure with multiple levels of porosity, from large scale originating in shrinkage of the template and formation of cracks between domains of PS spheres (see Fig. 1c), through actual IO structure and towards porosity in the wall of the inverted opal (Fig. 2b). The pores can be seen in a Fig. 2d, and are interspersed evenly in the structure of the inverted opal.

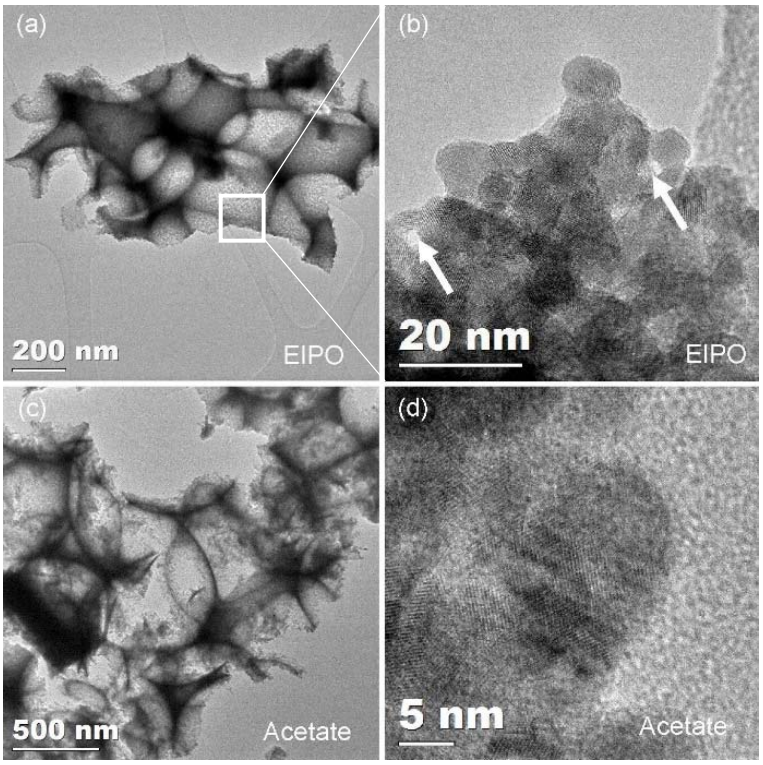

Figure 2. TEM images of inverted opals prepared from: (a-b) Tin ethylhexanoate-diisopropoxide. (c-d) Tin acetate (II).

Recently, we used cyclic voltammetry (CV) to observe processes occurring in indium oxide based alloying electrode, allowing observation of the processes occurring at the interface of two electrochemically active materials (23, 24). To examine the electrochemical lithiation processes occurring in tin oxide inverted opal electrodes, the as prepared IO structures were investigated by CV Samples were placed in stainless steel half-cells with lithium acting as counter and reference electrode. In this case, the anodic processes (discharge) refer to insertion of lithium into tin oxide active material, while cathodic part of the scan (discharge) refers to the removal of lithium from the host material. Characteristically, the first cycle consists of an irreversible process that can be related to formation of Solid Electrolyte Interphase (SEI) as well as reduction of tin oxide into metallic tin. This reaction is completed at ~1.25 V. Following that, the metallic tin alloys with lithium to form Li_xSn phases represented by a large peak in the cathodic part of the scan at ~0.5 V. In the anodic part of the cycle (charge) a large peak is present at ~0.7 V, related to the de-alloying of lithium and tin. The two peaks at 0.5 and 0.7 V in cathodic and anodic part of the cycle form the reversible insertion-removal reaction pair.

Additionally, a small peak present at about 1 V in the anodic part of the cycle can be related to re-oxidation of tin to its oxide. Usually this reaction is considered completely irreversible, however recent finding by Zhou et al. suggest that this reaction may be partially reversible (25). It does not however contribute to the increase in capacity of the battery.

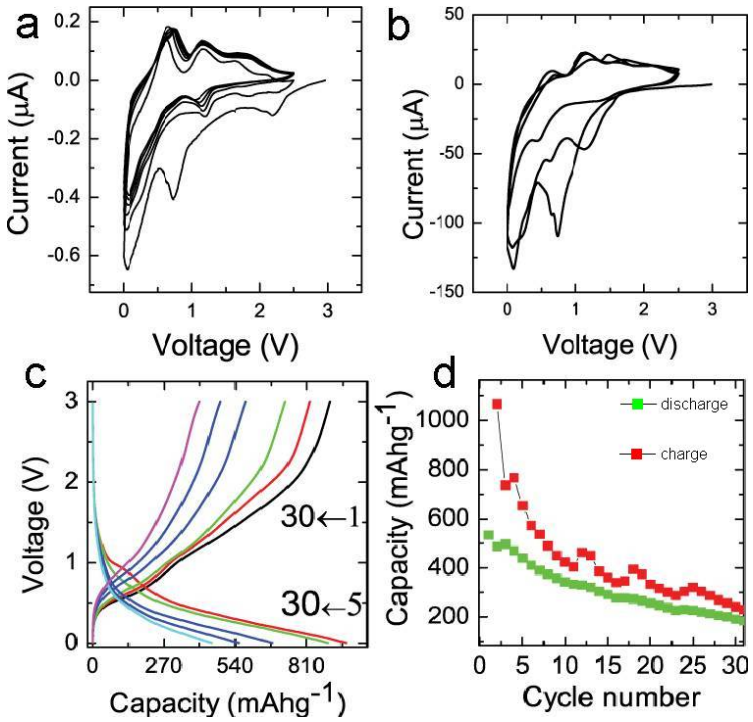

Figure 3. Cyclic voltammagrams for (a) IO from tin 2-methylhexano-isopropoxide. (b) IO from tin acetate (II). (c) Constant current charge-discharge response for IO from tin 2-methylhexano-isopropoxide over 30 cycles. (d) Cycle performance for an anode prepared from IO formed from tin 2-methylhexano-isopropoxide.

Constant current charge-discharge curves are present in Fig. 3c. Capacity fading is clearly present over 30 cycles, and is also highlighted in cycle lifetime plot presented in Figure 3d. The poor cycling stability of this material can be attributed to numerous processes. Firstly, volumetric expansion of tin oxide IO may cause cracking and pulverization of active material. Additionally, agglomeration of active material during cycling may cause closure of the pores formed in the inverted opal and prevent the electrolyte penetration of the electrode material. The initial discharge capacity loss between first and second cycle is related to the irreversible processes such as reduction of tin oxide to metallic tin and formation of solid electrolyte interphase. Recent reports suggest that lithium may deposit in pores provided by host material matrix. We suspect that this process might also be occurring in mesoporous inverted opals formed from tin alkoxide based precursors, however further investigation is needed in order to confirm these dependencies.

Conclusions

In summary, we prepared inverted opal structures from variety of precursors and showed that the type of precursor used greatly influences the morphology of the structures formed and has an influence on their electrochemical performance. These findings will be extended to fully characterize the dependence of the prepared structured on the precursor and the influence of the precursor and the structured porosity on the electrochemical performance as a Li-ion battery anode.

Acknowledgments
MO and EA acknowledge the support of the Irish Research Council under awards RS/2010/2170 and RS/2010/2920. The authors thank Prof. J. D. Holmes for access to the Electron Microscopy Analytical Facility at Tyndall National Institute. COD acknowledges support from Science Foundation Ireland under award no. 07/SK/B1232a, the UCC Strategic Research Fund, and from the Irish Research Council New Foundations Award.

References

1. P. G. Bruce, B. Scrosati and J.-M. Tarascon, *Angew. Chem. Int. Edit.*, **47**, 2930 (2008).
2. G. Wang, L. Zhang and J. Zhang, *Chem. Soc. Rev.*, **41**, 797 (2012).
3. Y. Wang, K. S. Chen, J. Mishler, S. C. Cho and X. C. Adroher, *Appl. Energy*, **88**, 981 (2011).
4. V. Etacheri, R. Marom, R. Elazari, G. Salitra and D. Aurbach, *Energy Environ. Sci.*, **4**, 3243 (2011).
5. U. Kasavajjula, C. S. Wang and A. J. Appleby, *J. Power Sources*, **163**, 1003 (2007).
6. H. Li, Z. X. Wang, L. Q. Chen and X. J. Huang, *Adv. Mater.*, 21, 4593 (2009).
7. J. W. Long, B. Dunn, D. R. Rolison and H. S. White, *Chem. Rev.*, **104**, 4463 (2004).
8. D. R. Rolison, J. W. Long, J. C. Lytle, A. E. Fischer, C. P. Rhodes, T. M. McEvoy, M. E. Bourg and A. M. Lubers, *Chem. Soc. Rev.*, **38**, 226 (2009).
9. N. Li and C. R. Martin, *J. Electrochem. Soc.*, **148,** A164 (2001).
10. A. Esmanski and G. A. Ozin, *Adv. Funct. Mater.*, **19**, 1999 (2009).
11. A. Stein, B. E. Wilson and S. G. Rudisill, *Chem. Soc. Rev.*, **42**, 2763 (2013).
12. J. L. Plawsky, J. K. Kim and E. F. Schubert, *Mater. Today*, **12**, 36 (2009).
13. J. H. Pikul, H. Gang Zhang, J. Cho, P. V. Braun and W. P. King, *Nat. Commun.*, **4**, 1732 (2013).
14. H. Zhang and P. V. Braun, *Nano Lett.*, **12**, 2778 (2012).
15. H. Zhang, X. Yu and P. V. Braun, *Nat. Nanotechnol.*, **6**, 277 (2011).
16. C. K. Chan, H. Peng, G. Liu, K. McIlwrath, X. F. Zhang, R. A. Huggins and Y. Cui, *Nat.Nanotechnol.*, **3**, 31 (2008).
17. A. M. Chockla, K. C. Klavetter, C. B. Mullins and B. A. Korgel, *ACS Appl. Mater. Interfaces*, **4**, 4658 (2012).
18. N. C. Li, C. R. Martin and B. Scrosati, *Electrochem. Solid State Lett.*, **3**, 316 (2000).
19. J. Zhang, Z. Chen, Z. Wang, W. Zhang and N. Ming, *Mater. Lett.*, **57**, 4466 (2003).
20. W. Khunsin, A. Amann, G. Kocher-Oberlehner, S. G. Romanov, S. Pullteap, H. C. Seat, E. P. O'Reilly, R. Zentel and C. M. Sotomayor Torres, *Adv. Funct. Mater.* **22**, 1812 (2012).
21. W. Khunsin, G. Kocher, S. G. Romanov and C. M. S. Torres, *Adv. Funct. Mater.*, **18**, 2471 (2008).
22. S. G. Romanov, M. Bardosova, I. M. Povey, M. E. Pemble and C. M. S. Torres, *Appl. Phys. Lett.*, **92**, 191106 (2008).
23. M. Osiak, W. Khunsin, E. Armstrong, T. Kennedy, C. M. S. Torres, K. M. Ryan and C. O'Dwyer, *Nanotechnology*, **24**, 065401 (2013).
24. M. Osiak, W. Khunsin, E. Armstrong, T. Kennedy, C. M. S. Torres, K. M. Ryan and C. O'Dwyer, *ECST Trans.*, **53**, 45 (2013).
25. G. Zhou, D. W. Wang, L. Li, N. Li, F. Li and H. M. Cheng, *Nanoscale*, **5**, 1576 (2013).